Urban Climate 42 (2022) 101124

Contents lists available at ScienceDirect

Urban Climate

journal homepage: www.elsevier.com/locate/uclim

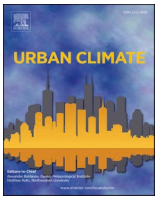

Intensification of sub-daily rainfall extremes in a low-rise urban area

Jamie Huang [a], Simone Fatichi [b], Giuseppe Mascaro [c], Gabriele Manoli [d], Nadav Peleg [e,*]

[a] Institute of Environmental Engineering, ETH Zurich, Zurich, Switzerland
[b] Department of Civil and Environmental Engineering, National University of Singapore, Singapore, Singapore
[c] School of Sustainable Engineering and the Built Environment, Arizona State University, Tempe, USA
[d] Department of Civil, Environmental & Geomatic Engineering, University College London, London, UK
[e] Institute of Earth Surface Dynamics, University of Lausanne, Lausanne, Switzerland

ARTICLE INFO

Keywords:
Urban rainfall intensification
Clausius–Clapeyron
Rainfall-temperature relation
Urban heat island
Dense rainfall network
Extreme rainfall intensity

ABSTRACT

Short-duration extreme rainfall events are the main trigger of flash and pluvial floods in cities. Depending on the local climate zone and urban fabric that affect meteorological variables such as air temperature, humidity, and aerosol concentration, the built environment can either intensify or reduce extreme rainfall intensity. This study examined how urbanization in a large metropolitan area characterized by open low-rise buildings, affected sub-daily extreme rainfall intensities over the period between 2000 and 2018. The research was conducted in the metropolitan region of Phoenix, Arizona, which is supported by a large and dense rain-gauge network (168 stations). The built area increased by 6% between 2001 and 2016 and the number of residences by 300,000. Over the study period, sub-daily extreme rainfall intensities intensified both in the urbanized area and in its rural surroundings but the intensification trend within the built area was considerably larger (3 times larger). We calculated a negative trend in aerosol concentration (-0.005 AOD y^{-1}) but a positive trend in near-surface air temperature that was considerably larger in the urban areas (0.15 °C y^{-1}) as compared to the rural counterpart (0.09 °C y^{-1}) for the period between 2005 and 2018. Although built surfaces and open low-rise buildings contributed to an increase in air temperature, they did not affect air humidity. Changes in rainfall extremes approximately follow the Clausius–Clapeyron relation within the urban area with an increase at a rate of 7% $°C^{-1}$. These results demonstrate that the warming effect associated with a low-rise urban area can cause an intensification of sub-daily rainfall extremes that is significantly larger than in nearby rural areas.

1. Introduction

Floods in cities are often caused by extreme rainfall events (Kundzewicz et al., 2014; Rosenzweig et al., 2018). Studies suggest that large metropolitan areas can act as intensifiers of extreme rainfall (Kishtawal et al., 2010; Holst et al., 2016; Niyogi et al., 2017; Shepherd et al., 2002; Singh et al., 2020; Yang et al., 2019a), leading to a greater extent and magnitude of floods (Huong and Pathirana,

* Corresponding author.
E-mail address: nadav.peleg@unil.ch (N. Peleg).

https://doi.org/10.1016/j.uclim.2022.101124
Received 4 September 2021; Received in revised form 15 December 2021; Accepted 4 February 2022
Available online 11 February 2022

2013; Miller and Hutchins, 2017). An example of this is the flooding that occurred in Houston as a result of Hurricane Harvey, which was greatly affected by the presence of the built environment (Zhang et al., 2018). Cities do not only modify the perviousness of the surface or influence storm extent but can also enhance short-duration (sub-daily) extreme rainfall intensities (Li et al., 2020; Yang et al., 2017b), which are the main triggers of urban pluvial floods (Hjelmstad et al., 2021).

The intensity of extreme urban rainfall can be affected by several factors, such as surface roughness, the presence of high-rise buildings, urban heat islands (UHI), enhanced sensible heat, and aerosol concentration (Han et al., 2014; Shephard, 2005). An increase in surface roughness in a city in comparison to its surroundings is associated with a slowing of the air masses that are advected toward the city, resulting in an enhanced surface moisture convergence that increases rainfall intensity (Debbage and Shepherd, 2019). In dense urban areas, high-rise buildings may enhance updrafts (Miao et al., 2011) and can create urban moisture islands (Wang et al., 2021), both of which can contribute to heavy rainfall. However, densely built areas can also lead to the dry island effect with unclear implications for rainfall intensities (Yang et al., 2017a). As a result of the UHI, the lower atmosphere over urban areas can be less stable, enhancing horizontal convergence and increasing the intensity of updraft and convective systems (Holst et al., 2016; Zhang et al., 2017). According to the Clausius-Clapeyron (CC) relation, a saturated atmosphere can hold approximately 7% more moisture per 1 °C increase in temperature (Lenderink and van Meijgaard, 2010; Molnar et al., 2015). Hence, assuming that the atmosphere is saturated during extreme rainfall events (Ali and Mishra, 2017; Mishra et al., 2012; Pan et al., 2019), UHIs are expected to contribute to an intensification of short-duration extremes (Wu et al., 2019). When aerosol concentrations are sufficiently high, they can act as a source of cloud condensation nuclei on which water can condense, enhancing cloud formation and precipitation; however, too elevated aerosols concentrations can also have the effect of slowing down the condensation of cloud water because smaller drops are generated, thus lowering the chances of drop precipitation (Han et al., 2014). A better understanding of how the urban fabric and Local Climate Zones (LCZ, Bechtel et al., 2015; Stewart and Oke, 2012; Wang et al., 2018) affect rainfall (e.g. Schmid and Niyogi, 2013; Zhu et al., 2019) is therefore needed to shed light on the relationship between urbanization and the processes that control extreme rainfall intensification.

Studies dealing with the intensification of urban rainfall usually rely on models rather than observations. The reason for this is that quantifying trends in extreme rainfall in cities is usually not an easy task, as in many cases, there are either not enough meteorological stations located within urban areas or the sample size is insufficient to conduct robust statistical analyses. In the past, just a few gauges were available per city for such an analysis (e.g. Hand and Shepherd (2009) in their study on Oklahoma City), and only recently more

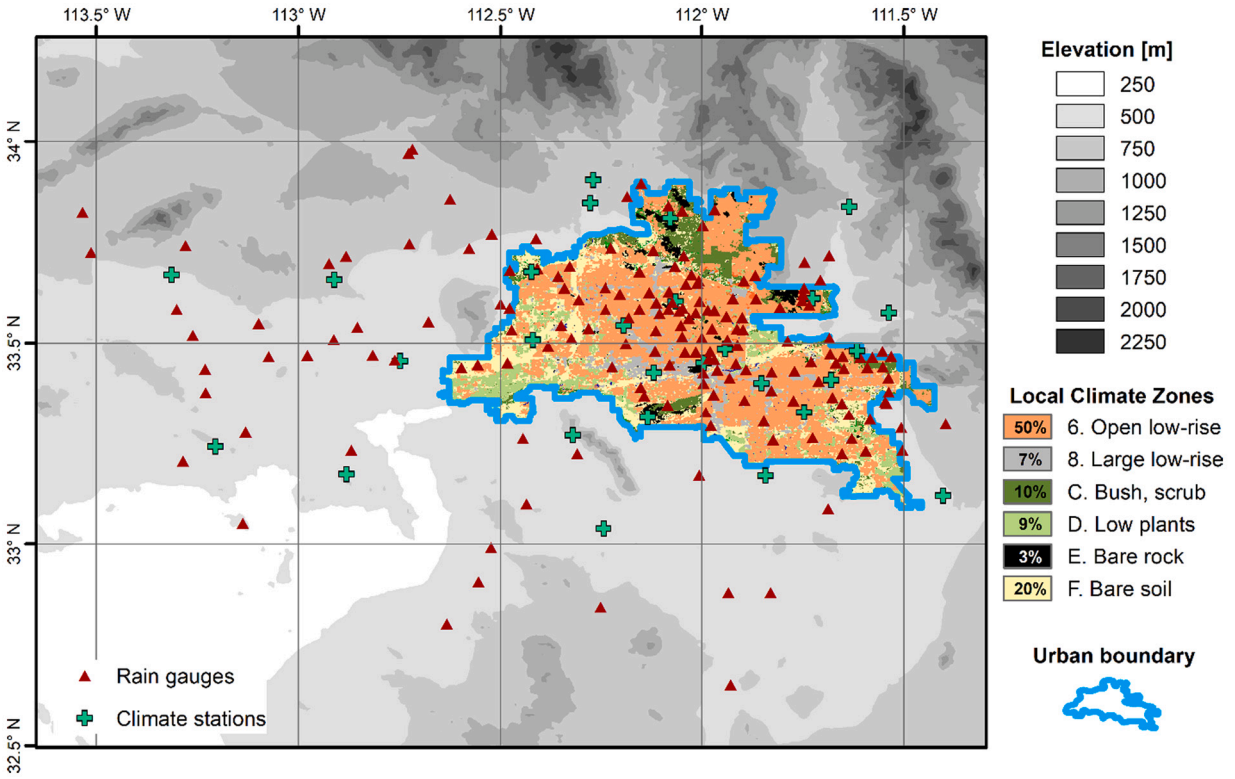

Fig. 1. A map showing the extent of the Phoenix metropolitan region (border with blue line) and its surroundings. Colors in the rural areas show the elevation changes (grayish colour scales) while the colors within the urban domain represent the Local Climate Zones (numbers within the legend of each LCZ indicate its relative contribution to the total urban area). Red triangles mark the locations of the 10-min rain-gauges (141) and green plus symbols mark the locations of the stations with also temperature sensors (27) showing the 168 rain-gauges used. (For interpretation of the references to colour in this figure legend, the reader is referred to the web version of this article.)

data is becoming available. Some examples are the analysis of urban rainfall conducted in the cities of Barcelona (23 rain gauges, Lana et al., 2020), Graz (22 rain gauges, Maier et al., 2020), Beijing (42 gauges, Yang et al., 2021) and Seoul (34 rain gauges, Yoon and Lee, 2017). A more detailed description of urban rainfall monitoring can be found in Cristiano et al. (2017).

Here, we addressed the question of intensification of extreme rainfall in an open low-rise metropolitan area using observations from a uniquely dense network of stations, which consists of 111 rain gauges covering the urban area of Phoenix, AZ and an additional 57 stations in the immediate rural surroundings. The first goal of this study is to investigate whether the built environment intensified extreme rainfall when compared to the rural counterpart in the last two decades. As we found an intensification, we examined if urban heat islands and/or aerosol concentrations contributed to the intensification of rainfall and whether there is any change of humidity in the urban area that could explain the observed changes in extreme rainfall.

2. Study area

The study area, located in Arizona (southwestern United States), consists of the urban agglomeration of Phoenix and its surroundings (Fig. 1). The urban area (4778 km^2) is comprised of several incorporated cities and is generally flat with some hilly terrain (mean elevation of 423 m and standard deviation of 115 m). The topography of the surroundings varies from mountains in the northeast reaching elevations of 2250 m to flat desert in the southwest with an elevation as low as 250 m (Fig. 1). The climate in the study area is classified as arid (BWh in the Köppen-Geiger Climate classes), meaning it is generally hot and has low precipitation throughout the year (Beck et al., 2018). There are two distinct rainfall seasons in the study area. The North American monsoon (Adams and Comrie, 1997) typically occurs from July through September and is characterized by heavy convective rainfall and summer thunderstorms that last less than 3 h. The second rainfall season occurs in the winter from December through March with frontal system storms of lower-intensity but longer duration (Mascaro, 2017).

CONUS-wide LCZ map elaborated by Demuzere et al. (2020a, 2020b), were used for the characterization of the urban surface cover. The Phoenix urban area is largely built (57% of the area) with 88% of it being open low-rise buildings and the rest being large low-rise buildings (LCZ 6 and 8, respectively, Fig. 1).

The metropolitan area has been one of the fastest-growing in the USA; its population increased from 2.9 million to 4.1 million residents between 2001 and 2019 (MAG, 2020). By examining impervious surface maps obtained from the National Land Cover Dataset (NLCD, Homer et al., 2004; Yang et al., 2018), one can see that the increase in population is also reflected in an increase in built area. The oldest NLCD 2001 dataset and the newest NLCD 2016 dataset (Fig. 2) provide an estimate of impervious cover between 0%

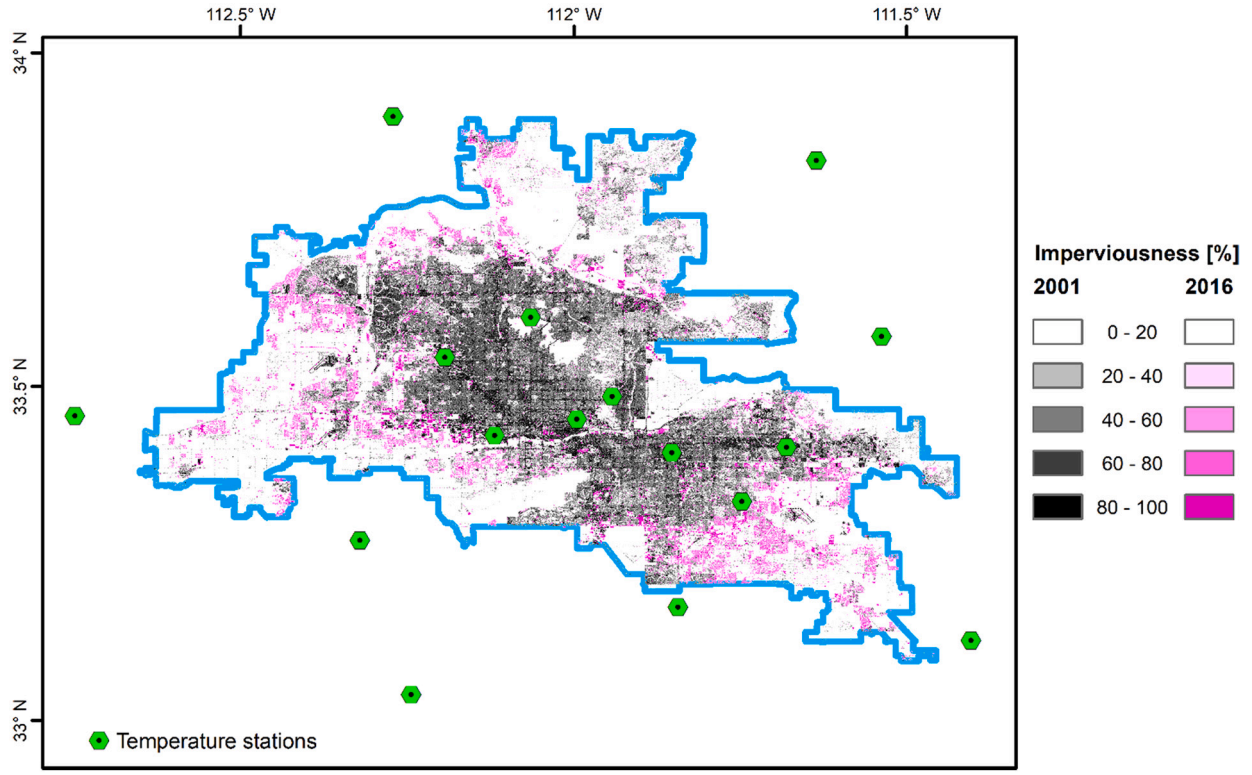

Fig. 2. A map of the Phoenix metropolitan region with the % of imperviousness reported for the year 2001 (blackish colour scale) and the % of imperviousness that was added by 2016 (purplish colour scale). Hexagons represent the locations of the 16 temperature stations within the urban domain and in its close surroundings.

(non-developed) and 100% (highly urban) and demonstrate that, during these 15 years, the average imperviousness increased from 16% to 24% with a substantial increase in the built area (Fig. 2).

A few long-term rainfall records (Shepherd, 2006) and numerical modeling (Yang et al., 2019a) have shown evidence of urban influences on rainfall intensity in and around the city. Georgescu et al. (2009b) used a numerical model to demonstrate how urbanization enhanced rainfall intensity in Phoenix between the 1970s and the early 21st century. They found that the increase in rainfall intensity is a result of enhancement of local convection, despite the fact that evapotranspiration, and therefore rainfall recycling, is reduced [Georgescu et al., 2012 further confirm this]. Moreover, further intensification of extreme daily rainfall intensities is expected toward the end of the century due to future urban development and climate change (Georgescu et al., 2021).

3. Data and methods

3.1. Rainfall, temperature and aerosols observations

Rainfall and temperature (air and dew point) data were obtained from the stations belonging to the Flood Control District of Maricopa County's Automated Local Evaluation in Real-Time (ALERT). The Phoenix metropolitan area and its surrounding areas have 357 stations with tipping buckets and 40 stations with temperature and humidity sensors. Some of the sensors archived measurements as far back as 1982, but most began operating in the late 1990s. In the following, only a short description of the monitoring network is provided as further details are described in Mascaro (2017).

The tipping buckets gauges, Hydrolynx model 5050P, measured rainfall at 1 mm per tip with a measurement error between 2% and 5% depending on the rainfall intensity. Rainfall data are processed and stored at 10 min resolution following the method presented in Mascaro et al. (2013) and Mascaro (2020) have been recently used it to compute rainfall extremes (Mascaro, 2020). For quality control, we removed missing data and high rainfall intensities (greater than 120 mm h^{-1}) if no rainfall was recorded in the preceding and following hour. We selected only stations within the elevation range of 300 m and 650 m to minimize the influence of orographic effects on rainfall intensity. Further, we only considered stations that had at least 15 years of complete annual rainfall records between 2000 and 2018. After quality control and selection, we were left with 111 stations in the urban area and 57 in the rural area (Fig. 1).

Near-surface air temperature (simply referred to as temperature hereafter) and dew point temperature are measured with the Vaisala HMP155 probe every 15 min. The estimated error in measurements is 0.4 °C for temperature and 3.6 °C for dew point temperature. The inverse distance weighting method was used to interpolate the temperature data from the 40 weather ALERT stations to each rain gauge.

The aerosol optical depth (AOD) measured at wavelength 550 nm is used as a proxy for the aerosol load in the atmosphere (Choudhury et al., 2020). The MODIS satellite sensors provide a global picture of AOD (Remer et al., 2008) at monthly resolution. AOD estimates were obtained from the NASA Earth Observations archives for TERRA/MODIS over the study area (a single grid cell of 0.1° × 0.1°, centered over Phoenix) for the period from March 2000 to February 2021.

3.2. Trend detection

Trends in extreme rainfall intensity were computed based on the annual maxima series. We fitted a simple linear regression and used the Theil-Sen slope estimation method to compute the trend. Afterward, we used the Mann-Kendall test to detect whether the trend is significant (Kendall, 1948; Mann, 1945), which is a common method for detecting trends in time series (Fatichi et al., 2009; Morin, 2011). Annual maxima values for the 10-minute time interval were obtained by simply extracting the maximum intensity value in each calendar year. We extracted the 1-hour duration annual maxima rainfall intensity values using a rolling average of six consecutive 10-minute time steps. All the rainfall measuring stations retained for the analysis were individually tested for trend.

Detecting whether a clear trend in extreme rainfall exists or not often requires long-term records (e.g. several decades; Morin, 2011; Farris et al., 2021). Detecting statistically significant trends in time series over 15 to 20 years (as in this study) is unlikely even when strong changes exist (Prosdocimi et al., 2014). To overcome this issue, we used an areal model that pools information across stations in the urban and rural regions. As a result, the statistical evidence of changes in extreme rainfall intensities is enhanced.

We used the areal model suggested by Prosdocimi et al. (2019). As a first step, we fitted a regression model using log-transformed annual maxima values with time as a covariate at each station. Then we used a Bayesian framework to estimate the area-specific trend signal and significance of the test statistic (Students' T-distribution with 2 degrees of freedom). Details on the model parameters and calibration procedure are presented in Prosdocimi et al. (2019), and in the R package by Prosdocimi and Dupont (2019).

In addition to extreme rainfall, trends were also calculated for temperature and AOD. We chose eight stations that measured the temperature within the urban area and eight stations that measured the temperature outside the urban area (Fig. 2) to calculate temperature trends. The analysis was based on the annual mean temperatures between 2005 and 2018 using linear regression and the Mann-Kendall test. We also analyzed the temperature trends during extreme rainfalls, which we defined as the average temperature 12 h before the occurrence of the annual maximum 10-min rainfall. Averaging the temperature 12 h before the extreme rainfall event is sufficient to represent the atmosphere thermodynamic during the development of the rainfall since most storms in the region last less than 2 h (Mascaro, 2017), and it is long enough to minimize the cooling effect of the strongest downdrafts. Using the same methodology, the trend for the mean annual AOD was calculated for the period between 2005 and 2020.

3.3. Extreme rainfall and temperature relation

To test the hypothesis of a CC relationship in the urban domain, the scaling rate between short-duration extreme rainfall intensities and temperature was calculated separately for the rural and urban areas. We calculated two sets of scaling rates for each station, one using temperature and the other one using dew point temperature (the latter was found to be more robust for analyzing rainfall scaling with a warming climate, as it filters humidity limitations, e.g. Ali and Mishra, 2017; Ali et al., 2021). Below we explain the computation of the scaling rate using temperature; the same procedure was used for dew point temperature unless stated otherwise. For more information on the method, see Ali et al. (2021) and references therein.

First, we classified all wet hours (rainfall intensity $\geq$ 0.1 mm h^{-1}) and associated temperatures at each rainfall station using the inverse distance weighting method to interpolate from the temperature observations. To minimize biases in the scaling rates caused either by elevation differences between the rainfall and temperature stations or by an excessive distance between them, we only chose rainfall stations that were within 3 km from the nearest temperature station. Thus, this analysis was limited to 38 rainfall stations, 20 of which are located within the urban area and 18 outside.

We then filtered the rainfall data to include only measurements where the temperature was greater than 4 °C (0 °C for dew point temperature) to eliminate any probability of solid precipitation in the data. Using fixed intervals of temperature (2 °C), we binned the rainfall data and calculated the 99th percentile (*P99*) of rainfall for each temperature bin. Only bins with at least 50 rainfall observations were included in the analysis. To eliminate biases in the scaling rate due to humidity limitations in the atmospheric column, which can be often observed at high temperatures above 25 °C (Peleg et al., 2018), we fitted a linear regression on the logarithm of *P99* and the mean temperature of each bin (*T*) from the first bin to the last bin before the breaking point (i.e. the bin with the highest *P99*):

$$logP99 = \alpha + \beta T \tag{1}$$

Then, we estimated the scaling $\frac{\partial P99}{\partial T}$ using an exponential transformation of the regression coefficient (β) given by (Ali et al., 2021):

$$\frac{\partial P99}{\partial T} = 100\left(e^{\beta} - 1\right) \tag{2}$$

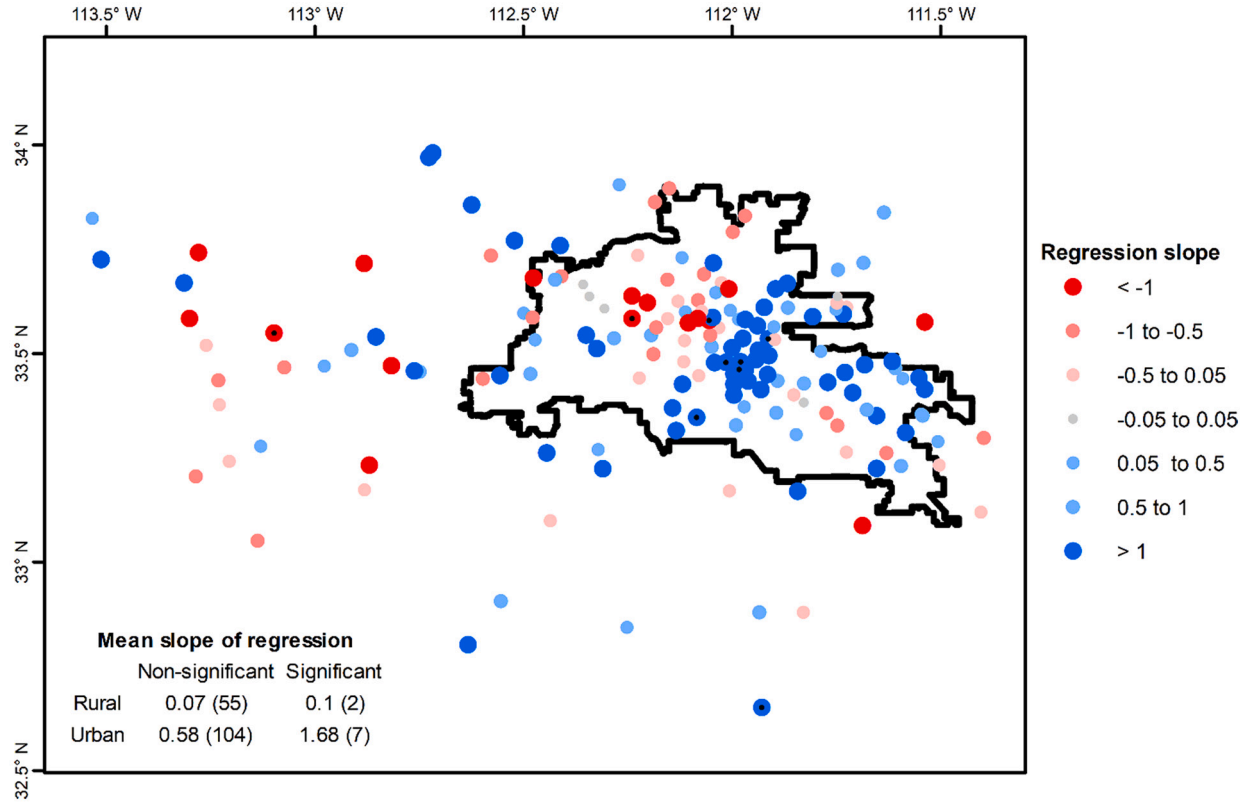

Fig. 3. Trends in maximum annual 10-min rainfall intensity [mm h^{-1} y^{-1}] between 2000 and 2018 computed with a simple linear regression. Red colors represent a negative trend while blue colors represent positive trends. The magnitude of the regression is also expressed by the symbol size. The mean values of the trends are summarized in the inset table (in brackets – the number of stations the value is computed for). Black dots mark stations with statistically significant regression (at 5% level). (For interpretation of the references to colour in this figure legend, the reader is referred to the web version of this article.)

In addition to the scaling analysis, we also correlated the intensity of the UHI with the diurnal timing of heavy rainfall. The eight urban stations and eight rural stations described in the previous section were used to calculate the diurnal cycle of the UHI as the difference between the mean urban and mean rural temperatures in each hour. We then used the stations located in the urban area to compute the percentage of occurrence of heavy rainfall intensity in each hour of the day. Heavy rainfall for this analysis is defined as rainfall exceeding the 90th percentile (P90).

3.4. Urban humidity analysis

In cases where the atmospheric moisture is not sufficient to saturate the air column, the intensity of short-duration extreme rainfall is not enhanced with increasing temperatures (Hardwick Jones et al., 2010). We extracted the information of the 99th percentile of dew point temperature (*DPT99*) against *T* using the same binning strategy as the one used to extract the *P99-T* relation, and plotted the *DPT99-T* relation for eight ground stations representing the urban area and eight ground stations representing the rural area (see Fig. 2 for the location of the stations). We then located the point of inflection where *DPT99* deviates from the 1:1 relationship between the two variables (Lenderink and van Meijgaard, 2010). The lower the temperature of the inflection point is, the more moisture-limitations are controlling the scaling of rainfall extreme with temperature entailing sub-CC rates rather than CC rates (e.g. Peleg et al., 2018). Urban and rural inflection points were detected and used as a proxy to determine whether the urban area exerts any control on the amount of humidity.

4. Results

4.1. Trends in rainfall extremes

Both in urban and rural areas, the majority of rainfall stations show a positive trend in extreme annual rainfall when computed with a simple linear regression, but the trends of annual maximum 10-min rainfall (Fig. 3) are larger than those at hourly scale (Fig. S1). On both the 10-min and hourly scales, there is a positive hotspot in the center of the urban area, as well as two negative hotspots, one in the urban area and one in the western rural area (Fig. 3 and Fig. S1). Slopes calculated with the Theil-Sen estimation method, have a similar magnitude to those obtained with the linear regression for the annual maximum 10-min rainfall (Fig. S2) and at the hourly scale (Fig. S3). Only 9 out of 168 rainfall stations showed statistically significant trends (at 5% level) at the 10-min scale and only 16 at the hourly scale. Nevertheless, the differences in the non-significant trends between the urban and rural areas are large enough (0.58 mm h^{-1} y^{-1} in the urban area versus 0.07 mm h^{-1} y^{-1} in the rural area, for the 10-min scale) to imply that extreme annual rainfall is intensifying at a higher rate in the urban area. For trends in extreme annual rainfall at the hourly scale, the pattern is similar, but with a smaller magnitude difference between the two regions (0.2 mm h^{-1} y^{-1} for the urban area versus 0.12 mm h^{-1} y^{-1} for the rural area).

Results of the trend analysis of the pooled data in the urban and rural areas statistically support the findings that extreme rainfall is intensifying at a larger rate in the urban domain compared to the rural area (Table 1). On both the 10-min and hourly scales, higher intensification rates were found in urban areas than in rural areas (positive trends in all cases), but the trends are only statistically significant in the urban area.

4.2. Extreme rainfall-temperature relationships

Both the 10-min and hourly scaling rates of P99 with T (Fig. 4a) are around the expected CC rate (i.e. 7% $°C^{-1}$). In the rural and urban areas, the scaling rates are similar with medians (and standard deviations) of 6.1(0.93)% $°C^{-1}$ and 6.3(1.24)% $°C^{-1}$ at the 10-min scale, and medians of 6.4(1.14)% $°C^{-1}$ and 7.2(1.09)% $°C^{-1}$ at the hourly scale, respectively. P99 scaling rates using DPT are higher than those obtained with T (Fig. 4b). However, also in this case, the differences between urban and rural scaling rates are small and very close to the expected CC rate [6.7(1.9)% $°C^{-1}$ and 7.7(1.78)% $°C^{-1}$ for the 10-min scale and 8.9(1.35)% $°C^{-1}$ and 9.2(2.13)% $°C^{-1}$ for the hourly scale; rural and urban, respectively]. A two-sample Kolmogorov-Smirnov test was used to compare the scaling rates between the urban and rural areas and a significant difference (at 5% significance level) was only found in the hourly P99-T relation.

4.3. Trends in temperature and aerosols

An increase in temperatures was observed in both rural and urban areas (Fig. 5a). Using a 5-year moving window, the average temperature was found to remain relatively unchanged between 2000 and 2005 but it increases thereafter. The trend in annual temperature between 2005 and 2018 was higher in the urban area (0.15 °C y^{-1}) than in the rural area (0.09 °C y^{-1}). Mann-Kendall test

Table 1
Regional trends [mm h^{-1} y^{-1}] in annual maximum 10-min and hourly rainfall intensity in urban and rural regions.

Region	Duration	Posterior mean of trend	Significant trend
Urban	10 min	0.53	Yes
	1 h	0.6	Yes
Rural	10 min	0.18	No
	1 h	0.2	No

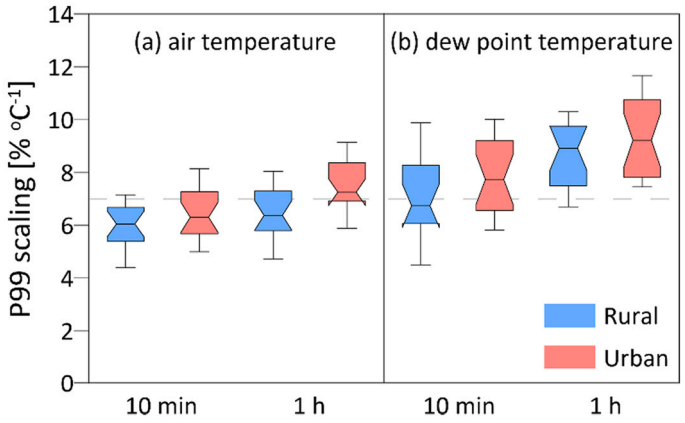

Fig. 4. Box-plots of 10-min and hourly extreme rainfall intensity (99th percentile, P99) scaling with temperature for the rain-gauges located in urban (red, 20 stations) and rural (blue, 18 stations) areas. The scaling is computed with air temperature (a) and with dew point temperature (b). The dashed line represents the theoretical ≈7% °C^{-1} extreme rainfall intensification rate obtained from the Clausius–Clapeyron relation. (For interpretation of the references to colour in this figure legend, the reader is referred to the web version of this article.)

results indicate that both trends are statistically significant (p-values are <0.01 and 0.02, respectively). Also, urban temperature increases during extreme rainfalls are higher (0.26 °C y^{-1}) than rural temperature increases (0.14 °C y^{-1}) although neither trend is statistically significant (p-values of 0.27 and 0.66, respectively).

The DPT99 and T values are similar in both the urban and rural areas, with the inflection point located at 16 °C (Fig. 5b). At three of the temperature bins, the DPT in the rural area is greater than in the urban area (at the bin of 15–17 °C: DPT99 is greater by 0.4 °C; 21–23 °C: by 0.8 °C; and 23–25 °C: by 0.4 °C). Since the difference in DPT99 is small and not seen in all temperature bins, it remains inconclusive if humidity is suppressed over the urban domain when compared to the rural areas during these extreme events.

Aerosol concentrations decreased in the study area (Fig. 5c). We found that, similar to the trends in temperature, the AOD remained stable from 2000 to 2005, but subsequently decreased. The AOD trend between 2005 and 2018 is −0.005 AOD y^{-1}, and it is statistically significant with a p-value <0.01.

The diurnal cycles of UHI and heavy rainfall occurrences are presented in Fig. 6. UHI intensity is lowest at 8 am (less than 0.1 °C) and steadily increases to its maximum intensity of 0.9 °C at 8 pm. Heavy rainfall intensities are less common during low UHI intensity (6 am to 10 am, 15.3% of $P > P90$ occurrences) than during high UHI intensity (6 pm to 10 pm, 29.5%). Maximum UHI intensity occurs at the same time as the highest frequency of rainfall events above the P90.

5. Discussion and implications

In the last two decades, both the urban area and rural surroundings of the Phoenix metropolitan region have experienced on average an increase in sub-daily extreme rainfall (Fig. 3 and Table 1), but the increase has been considerably larger in the urban area. An extreme precipitation intensification in urban areas larger than their surroundings has been also reported in other cities (e.g. Shastri et al., 2015; Yang et al., 2021; Yoon and Lee, 2017). The dense rain-gauge network used in our study area, however, enables a robust statistical analysis of extreme rainfall trends that is unique and goes beyond the existing results presented in previous studies.

Intensification of sub-daily extreme rainfall intensities is positively correlated with (and likely mostly driven by) increasing temperatures (Fig. 4). The Phoenix metropolitan region showed a higher temperature trend in the urban area than in the rural surroundings for both the annual temperature (Fig. 5a) and the 12-hour average temperature prior to extreme rainfall events. This is most likely the result of the development of a UHI (Manoli et al., 2019) triggered by the massive urbanization of the city over the past two decades (Debbage and Shepherd, 2015; Yang et al., 2019a), as the UHI did not occur in the early 2000s (Georgescu et al., 2011). Most heavy rainfall intensities also occur at the same time as the maximum UHI (Fig. 6). We can rule out influences from aerosols and humidity on extreme rainfall intensification because AOD exhibited a negative trend during the last two decades (Fig. 5c), and we did not find evidence in the analyzed dataset that air humidity is suppressed or enhanced over the Phoenix urban area (Fig. 5b). One aspect we have not explored is how changes in land use affect local convection and rainfall, and in particular how changes in irrigation patterns inside and outside the city affect these processes. In the last 30 years of the 20th century, surface energy budgets in Phoenix region have changed considerably as a result of changes in irrigation patterns (Georgescu et al., 2008, 2009a), which have affected rainfall recycling, intensification, and distribution (Georgescu et al., 2009b; Yang et al., 2019b). However, the total irrigated areas for agriculture in Arizona have declined only slightly since the turn of the 21st century, which is the study period considered here (Elias et al., 2016). Plus, a recent modeling study by Yang et al. (2019b) showed that urban irrigation has not significantly modified rainfall accumulations but has changed its spatial distribution.

There was no significant difference in rainfall scaling rates between urban and rural areas, which are both following expectations from the CC relationship (Fig. 4). This is an indication that thermodynamic controls related to the increase in air temperature rather than atmospheric dynamic controls related to changes in surface roughness, convection potential, or moisture convergence are the

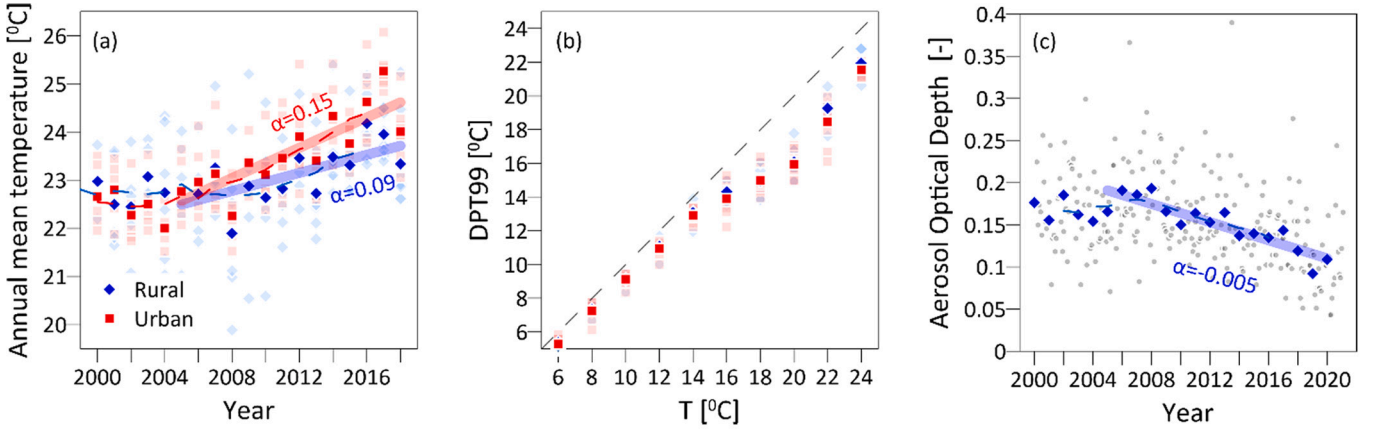

Fig. 5. (a) Annual mean temperature of the urban (light red squares) and rural (light blue diamonds) climate stations presented in Fig. 2. Dark red squares and dark blue diamonds represent the average annual mean temperature for the urban and rural areas (respectively). The dashed blue and red lines represent the 5-year moving window average. Thick blue (urban) and red (rural) lines are the linear trends (α is the slope) computed for the period 2005–2018. (b) 99th percentile dew point temperature (DPT99) – air temperature (T) plot for the same climate stations (light red - urban, light blue - rural). Dark symbols represent the urban (red) and rural (blue) averages for each temperature bin. (c) Monthly Aerosol Optical Depth (AOD) estimates over the Phoenix metropolitan area (gray dots). The dashed blue line represents the 5-year moving window average for the mean annual AOD (blue diamonds). The thick blue line is the linear trend (α is the slope) computed for the period 2005–2020. (For interpretation of the references to colour in this figure legend, the reader is referred to the web version of this article.)

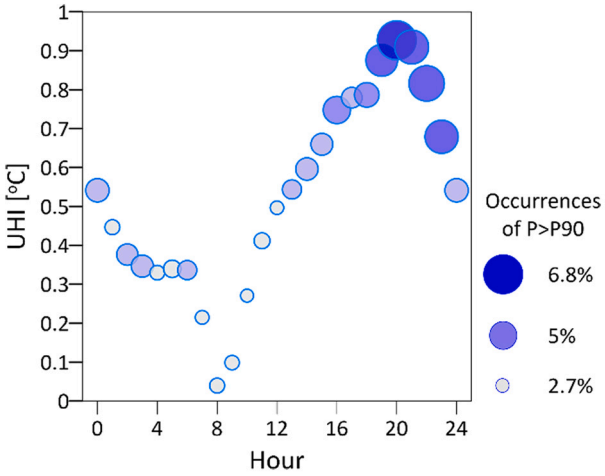

Fig. 6. The diurnal cycle of UHI. The size of the symbols shows the diurnal distribution of the occurrences of rainfall intensity (P) above the 90th percentile (P90).

main contributing factors for the observed three-fold increase in annual maximum 10-min and hourly rainfall intensity over the Phoenix urban area when compared to the rural surrounding (Table 1). Similarity of rainfall extreme scaling rates between urban and rural areas are in line with the findings of a few other studies: Mishra et al. (2012) for US cities, Ali and Mishra (2017) for Indian cities, and Pan et al. (2019) for cities in south China. However, our analysis differs from such studies as we used data from multiple stations to compare rainfall scaling rates in a single metropolitan area, while previous studies only analyzed rainfall scaling rates using a single or a few stations per city.

The Phoenix metropolitan region is located in a dry climate and is mainly characterized by open low-rise buildings (LCZ 6, Fig. 1). The results of our analysis are likely to be valid in other cities located in semi-arid climates that are characterized by similar urban fabrics, such as other metropolitan areas in the southwest US, but their transferability to different urban settings and climatic regions remains a subject for future enquiries.

Assuming that the scaling rate of extreme rainfall with temperature in urban areas will follow the CC rate, as it seems to occur in large parts of the globe when humidity limitations are filtered out (Ali et al., 2018, 2021), and considering the changes in temperature due to climate change and urbanization, it is theoretically possible to extrapolate the magnitude of changes in sub-daily extreme rainfall intensities in cities in the future. This also implies that rainfall extremes will intensify more in cities with larger UHI effects, even though the relation between mean UHI and UHI during extreme rainfall might be more complex than found here. This simple scaling with temperature assumption might not hold if the humidity in the future becomes a strong limiting factor – especially at very high temperatures, if the aerosols load increases considerably, and if global warming impacts the large-scale circulation (Fowler et al., 2021; Peleg et al., 2018), strongly modifying rainfall patterns. In cities with high aerosol emissions, high-rise buildings (LCZ 4) with enhanced convection, and compact high- to mid-rise buildings (LCZ 1 and 2) that can act as a barrier to humidity transport, deviations from the CC scaling rate could occur or are at least expected. Further research is needed to better understand how local climate zones affect rainfall scaling rates and extreme rainfall intensification. However, such a simple relation between temperature and rainfall extremes can be used as a first-order approximation of “expected changes” in local rainfall extremes at short durations as those are anyhow characterized by a very large stochastic uncertainty (Fatichi et al., 2016; Peleg et al., 2019).

6. Conclusions

We used 168 rain gauges and 40 temperature sensors to analyze the changes in extreme rainfall intensities in the Phoenix metropolitan area. In the urban area, rainfall extremes intensify at a much higher rate than its rural surroundings. The scaling rate between sub-daily extreme rainfall intensity and temperature was found to roughly follow the theoretical Clausius-Clapeyron scaling rate of 7% $^{\circ}C^{-1}$ in the urban and rural areas. For this reason, we concluded that the enhanced rainfall intensity is a consequence of the larger increase in air temperature in the city, which has increased significantly more than in the rural areas in the last two decades likely because of urbanization. Other than the change in urban temperature, we have not noticed any considerable changes in humidity or increase in aerosol levels that would affect dynamic storm properties. Based on the observed rainfall scaling rate, a simple extrapolation of the intensification of sub-daily extreme rainfall intensities would be possible based on thermodynamic arguments in similar urban fabrics and climates for various warming and urban heat island scenarios. However, this represents only a first-order approximation of changes in rainfall extremes and more analyses are needed to understand if different urban morphologies can impart a signature on storm dynamics and rainfall extremes.

CRediT authorship contribution statement

Jamie Huang: Methodology, Formal analysis, Investigation, Visualization, Writing – original draft, Writing – review & editing. **Simone Fatichi:** Conceptualization, Methodology, Writing – original draft, Writing – review & editing. **Giuseppe Mascaro:** Conceptualization, Methodology, Resources, Writing – original draft, Writing – review & editing. **Gabriele Manoli:** Conceptualization, Methodology, Writing – original draft, Writing – review & editing. **Nadav Peleg:** Conceptualization, Methodology, Formal analysis, Visualization, Supervision, Writing – original draft, Writing – review & editing.

Declaration of Competing Interest

None.

Acknowledgments

We thank three anonymous reviewers for their insightful comments that helped to improve the quality of our manuscript. Nadav Peleg acknowledges the support of the Swiss National Science Foundation (SNSF), Grant 194649 ("Rainfall and floods in future cities"). Giuseppe Mascaro acknowledges the support by the National Science Foundation (NSF) Award "SCC: Community-Based Automated Information for Urban Flooding" (Award 1831475). Gabriele Manoli acknowledges support by the "The Branco Weiss Fellowship - Society in Science" administered by ETH Zurich.

Appendix A. Supplementary data

Supplementary data to this article can be found online at https://doi.org/10.1016/j.uclim.2022.101124.

References

Adams, D.K., Comrie, A.C., 1997. The north American monsoon. Bull. Am. Meteorol. Soc. 78 (10), 2197–2214. https://doi.org/10.1175/1520-0477(1997)078<2197:TNAM>2.0.CO;2.

Ali, H., Mishra, V., 2017. Contrasting response of rainfall extremes to increase in surface air and dewpoint temperatures at urban locations in India. Sci. Rep. 7 https://doi.org/10.1038/s41598-017-01306-1.

Ali, H., Fowler, H.J., Mishra, V., 2018. Global observational evidence of strong linkage between dew point temperature and precipitation extremes. Geophys. Res. Lett. 45 (22), 12,320–12,330. https://doi.org/10.1029/2018GL080557.

Ali, H., Peleg, N., Fowler, H., 2021. Global scaling of rainfall with dewpoint temperature reveals considerable ocean-land difference. Geophys. Res. Lett. 48, e2021GL093798 https://doi.org/10.1029/2021GL093798.

Bechtel, B., et al., 2015. Mapping local climate zones for a worldwide database of the form and function of cities. ISPRS Int. J. Geo Inf. 4 (1), 199–219.

Beck, H.E., et al., 2018. Present and future Köppen-Geiger climate classification maps at 1-km resolution. Sci. Data 5 (1), 180214. https://doi.org/10.1038/sdata.2018.214.

Choudhury, G., et al., 2020. Aerosol-enhanced high precipitation events near the Himalayan foothills. Atmos. Chem. Phys. 20 (23), 15389–15399. https://doi.org/10.5194/acp-20-15389-2020.

Cristiano, E., ten Veldhuis, M.C., van De Giesen, N., 2017. Spatial and temporal variability of rainfall and their effects on hydrological response in urban areas - a review. Hydrol. Earth Syst. Sci. 21 (7), 3859–3878. https://doi.org/10.5194/hess-21-3859-2017.

Debbage, N., Shepherd, J.M., 2015. The urban heat island effect and city contiguity. Comput. Environ. Urban. Syst. 54, 181–194. https://doi.org/10.1016/j.compenvurbsys.2015.08.002.

Debbage, N., Shepherd, J.M., 2019. Urban influences on the spatiotemporal characteristics of runoff and precipitation during the 2009 Atlanta flood. J. Hydrometeorol. 20 (1), 3–21. https://doi.org/10.1175/jhm-d-18-0010.1.

Demuzere, M., et al., 2020a. Combining expert and crowd-sourced training data to map urban form and functions for the continental US. Sci. Data 7 (1), 264. https://doi.org/10.1038/s41597-020-00605-z.

Demuzere, M., et al., 2020b. CONUS-wide LCZ Map and Training Areas. https://doi.org/10.6084/m9.figshare.11416950.v1.

Elias, E., Rango, A., Smith, R., Maxwell, C., Steele, C., Havstad, K., 2016. Climate change, agriculture and water resources in the southwestern United States. J. Contemp. Water Res. Educ. 158 (1), 46–61. https://doi.org/10.1111/j.1936-704X.2016.03218.x.

Farris, S., Deidda, R., Viola, F., Mascaro, G., 2021. On the role of serial correlation and field significance in detecting changes in extreme precipitation frequency. Water Resour. Res. 57 https://doi.org/10.1029/2021WR030172 e2021WR030172.

Fatichi, S., Barbosa, S.M., Caporali, E., Silva, M.E., 2009. Deterministic versus stochastic trends: detection and challenges. J. Geophys. Res. Atmos. 114 (D18) https://doi.org/10.1029/2009JD011960.

Fatichi, S., Ivanov, V.Y., Paschalis, A., Peleg, N., Molnar, P., Rimkus, S., Kim, J., Burlando, P., Caporali, E., 2016. Uncertainty partition challenges the predictability of vital details of climate change. Earth's Future 4 (5), 240–251. https://doi.org/10.1002/2015EF000336.

Fowler, H.J., Lenderink, G., Prein, A.F., Westra, S., Allan, R.P., Ban, N., Barbero, R., Berg, P., Blenkinsop, S., Do, H.X., Guerreiro, S., Haerter, J.O., Kendon, E.J., Lewis, E., Schaer, C., Sharma, A., Villarini, G., Wasko, C., Zhang, X., 2021. Anthropogenic intensification of short-duration rainfall extremes. Nat. Rev. Earth Environ. 2 (2), 107–122. https://doi.org/10.1038/s43017-020-00128-6.

Georgescu, M., Miguez-Macho, G., Steyaert, L.T., Weaver, C.P., 2008. Sensitivity of summer climate to anthropogenic land-cover change over the Greater Phoenix, AZ, region. J. Arid Environ. 72 (7), 1358–1373. https://doi.org/10.1016/j.jaridenv.2008.01.004.

Georgescu, M., Miguez-Macho, G., Steyaert, L.T., Weaver, C.P., 2009a. Climatic effects of 30 years of landscape change over the Greater Phoenix, Arizona, region: 1. Surface energy budget changes. J. Geophys. Res. Atmos. 114 (D5) https://doi.org/10.1029/2008JD010745.

Georgescu, M., Miguez-Macho, G., Steyaert, L.T., Weaver, C.P., 2009b. Climatic effects of 30 years of landscape change over the Greater Phoenix, Arizona, region: 2. Dynamical and thermodynamical response. J. Geophys. Res. Atmos. 114 (D5) https://doi.org/10.1029/2008JD010762.

Georgescu, M., Moustaoui, M., Mahalov, A., Dudhia, J., 2011. An alternative explanation of the semiarid urban area "oasis effect". J. Geophys. Res. Atmos. 116 (D24) https://doi.org/10.1029/2011JD016720.

Georgescu, M., Mahalov, A., Moustaoui, M., 2012. Seasonal hydroclimatic impacts of Sun Corridor expansion. Environ. Res. Lett. 7 (3), 034026 https://doi.org/10.1088/1748-9326/7/3/034026.
Georgescu, M., Broadbent, A.M., Wang, M., Krayenhoff, E.S., Moustaoui, M., 2021. Precipitation response to climate change and urban development over the continental United States. Environ. Res. Lett. 16 (4), 044001 https://doi.org/10.1088/1748-9326/abd8ac.
Han, J.Y., Baik, J.J., Lee, H., 2014. Urban impacts on precipitation. Asia-Pac. J. Atmos. Sci. 50 (1), 17–30. https://doi.org/10.1007/s13143-014-0016-7.
Hand, L.M., Shepherd, J.M., 2009. An investigation of warm-season spatial rainfall variability in Oklahoma City: possible linkages to urbanization and prevailing wind. J. Appl. Meteorol. Climatol. 48 (2), 251–269. https://doi.org/10.1175/2008jamc2036.1.
Hardwick Jones, R., Westra, S., Sharma, A., 2010. Observed relationships between extreme sub-daily precipitation, surface temperature, and relative humidity. Geophys. Res. Lett. 37 (22) https://doi.org/10.1029/2010GL045081.
Hjelmstad, A., Shrestha, A., Garcia, M., Mascaro, G., 2021. Propagation of radar rainfall uncertainties into urban pluvial flood modeling during the North American monsoon. Hydrol. Sci. J. 66 (15), 2232–2248. https://doi.org/10.1080/02626667.2021.1980216.
Holst, C.C., Tam, C.-Y., Chan, J.C.L., 2016. Sensitivity of urban rainfall to anthropogenic heat flux: a numerical experiment. Geophys. Res. Lett. 43 (5), 2240–2248. https://doi.org/10.1002/2015GL067628.
Homer, C., Huang, C., Yang, L., Wylie, B., Coan, M., 2004. Development of a 2001 National Land-Cover Database for the United States. Photogramm. Eng. Remote. Sens. 70 (7), 829–840. https://doi.org/10.14358/PERS.70.7.829.
Huong, H.T.L., Pathirana, A., 2013. Urbanization and climate change impacts on future urban flooding in Can Tho city, Vietnam. Hydrol. Earth Syst. Sci. 17 (1), 379–394. https://doi.org/10.5194/hess-17-379-2013.
Kendall, M.G., 1948. Rank correlation methods. In: Rank Correlation Methods. Griffin, Oxford, England.
Kishtawal, C.M., Niyogi, D., Tewari, M., Pielke, R.A., Shepherd, J.M., 2010. Urbanization signature in the observed heavy rainfall climatology over India. Int. J. Climatol. 30 (13), 1908–1916. https://doi.org/10.1002/joc.2044.
Kundzewicz, Z.W., et al., 2014. Flood risk and climate change: global and regional perspectives. Hydrol. Sci. J. 59 (1), 1–28. https://doi.org/10.1080/02626667.2013.857411.
Lana, X., et al., 2020. Characterization of standardized heavy rainfall profiles for Barcelona city: clustering, rain amounts and intensity peaks. Theor. Appl. Climatol. 142 (1–2), 255–268. https://doi.org/10.1007/s00704-020-03315-z.
Lenderink, G., van Meijgaard, E., 2010. Linking increases in hourly precipitation extremes to atmospheric temperature and moisture changes. Environ. Res. Lett. 5 (2), 025208 https://doi.org/10.1088/1748-9326/5/2/025208.
Li, Y.F., et al., 2020. Strong intensification of hourly rainfall extremes by urbanization. Geophys. Res. Lett. 47 (14) https://doi.org/10.1029/2020gl088758.
MAG, 2020. MAG Fast Facts - Population and Growth. https://webadmin.azmag.gov/About-Us/Divisions/Regional-Analytics-Division/MAG-Fast-Facts-Population-and-Growth (last accessed: 12/07/2021).
Maier, R., Krebs, G., Pichler, M., Muschalla, D., Gruber, G., 2020. Spatial rainfall variability in urban environments-high-density precipitation measurements on a city-scale. Water 12 (4). https://doi.org/10.3390/w12041157.
Mann, H.B., 1945. Nonparametric tests against trend. Econometrica 13 (3), 245–259. https://doi.org/10.2307/1907187.
Manoli, G., Fatichi, S., Schläpfer, M., Yu, K., Crowther, T.W., Meili, N., Burlando, P., Katul, G.G., Bou-Zeid, E., 2019. Magnitude of urban heat islands largely explained by climate and population. Nature 573 (7772), 55–60.
Mascaro, G., 2017. Multiscale spatial and temporal statistical properties of rainfall in Central Arizona. J. Hydrometeorol. 18 (1), 227–245. https://doi.org/10.1175/JHM-D-16-0167.1.
Mascaro, G., 2020. Comparison of local, regional, and scaling models for rainfall intensity–duration–frequency analysis. J. Appl. Meteorol. Climatol. 59 (9), 1519–1536. https://doi.org/10.1175/jamc-d-20-0094.1.
Mascaro, G., Deidda, R., Hellies, M., 2013. On the nature of rainfall intermittency as revealed by different metrics and sampling approaches. Hydrol. Earth Syst. Sci. 17, 1–15. https://doi.org/10.5194/hess- 17-1-2013.
Miao, S.G., Chen, F., Li, Q.C., Fan, S.Y., 2011. Impacts of urban processes and urbanization on summer precipitation: a case study of heavy rainfall in Beijing on 1 August 2006. J. Appl. Meteorol. Climatol. 50 (4), 806–825. https://doi.org/10.1175/2010jamc2513.1.
Miller, J.D., Hutchins, M., 2017. The impacts of urbanisation and climate change on urban flooding and urban water quality: a review of the evidence concerning the United Kingdom. J. Hydrol. Region. Stud. 12, 345–362. https://doi.org/10.1016/j.ejrh.2017.06.006.
Mishra, V., Wallace, J.M., Lettenmaier, D.P., 2012. Relationship between hourly extreme precipitation and local air temperature in the United States. Geophys. Res. Lett. 39 https://doi.org/10.1029/2012gl052790.
Molnar, P., Fatichi, S., Gaál, L., Szolgay, J., Burlando, P., 2015. Storm type effects on super Clausius–Clapeyron scaling of intense rainstorm properties with air temperature. Hydrol. Earth Syst. Sci. 19 (4), 1753–1766. https://doi.org/10.5194/hess-19-1753-2015.
Morin, E., 2011. To know what we cannot know: global mapping of minimal detectable absolute trends in annual precipitation. Water Resour. Res. 47 (7) https://doi.org/10.1029/2010WR009798.
Niyogi, D., Lei, M., Kishtawal, C., Schmid, P., Shepherd, M., 2017. Urbanization impacts on the summer heavy rainfall climatology over the eastern United States. Earth Interact. 21 https://doi.org/10.1175/ei-d-15-0045.1.
Pan, C.L., Wang, X.W., Liu, L., Wang, D.S., Huang, H.B., 2019. Characteristics of heavy storms and the scaling relation with air temperature by event process-based analysis in South China. Water 11 (2). https://doi.org/10.3390/w11020185.
Peleg, N., et al., 2018. Intensification of convective rain cells at warmer temperatures observed from high-resolution weather radar data. J. Hydrometeorol. 19 (4), 715–726. https://doi.org/10.1175/jhm-d-17-0158.1.
Peleg, N., Molnar, P., Burlando, P., Fatichi, S., 2019. Exploring stochastic climate uncertainty in space and time using a gridded hourly weather generator. J. Hydrol. 571, 627–641. https://doi.org/10.1016/j.jhydrol.2019.02.010.
Prosdocimi, I., Dupont, E., 2019. R Scripts Underlying the Article “Areal Models for Spatially Coherent Trend Detection: The Case of British Peak River Flows” https://doi.org/10.5281/zenodo.3497404.
Prosdocimi, I., Kjeldsen, T.R., Svensson, C., 2014. Non-stationarity in annual and seasonal series of peak flow and precipitation in the UK. Nat. Hazards Earth Syst. Sci. 14 (5), 1125–1144. https://doi.org/10.5194/nhess-14-1125-2014.
Prosdocimi, I., et al., 2019. Areal models for spatially coherent trend detection: the case of British Peak River flows. Geophys. Res. Lett. 46 (22), 13054–13061. https://doi.org/10.1029/2019GL085142.
Remer, L.A., et al., 2008. Global aerosol climatology from the MODIS satellite sensors. J. Geophys. Res. Atmos. 113 (D14) https://doi.org/10.1029/2007JD009661.
Rosenzweig, B.R., McPhillips, L., Chang, H., Cheng, C., Welty, C., Matsler, M., Iwaniec, D., Davidson, C.I., 2018. Pluvial flood risk and opportunities for resilience. WIREs Water 5 (6), e1302. https://doi.org/10.1002/wat2.1302.
Schmid, P.E., Niyogi, D., 2013. Impact of city size on precipitation-modifying potential. Geophys. Res. Lett. 40 (19), 5263–5267. https://doi.org/10.1002/grl.50656.
Shastri, H., Paul, S., Ghosh, S., Karmakar, S., 2015. Impacts of urbanization on Indian summer monsoon rainfall extremes. J. Geophys. Res.-Atmos. 120 (2), 495–516. https://doi.org/10.1002/2014jd022061.
Shephard, J.M., 2005. A review of current investigations of urban-induced rainfall and recommmendations for the future. Earth Interact. 9.
Shepherd, J.M., 2006. Evidence of urban-induced precipitation variability in arid climate regimes. J. Arid Environ. 67 (4), 607–628. https://doi.org/10.1016/j.jaridenv.2006.03.022.
Shepherd, J.M., Pierce, H., Negri, A.J., 2002. Rainfall modification by major urban areas: observations from spaceborne rain radar on the TRMM satellite. J. Appl. Meteorol. 41 (7), 689–701. https://doi.org/10.1175/1520-0450(2002)041<0689:Rmbmua>2.0.Co;2.
Singh, J., Karmakar, S., PaiMazumder, D., Ghosh, S., Niyogi, D., 2020. Urbanization alters rainfall extremes over the contiguous United States. Environ. Res. Lett. 15 (7) https://doi.org/10.1088/1748-9326/ab8980.
Stewart, I.D., Oke, T.R., 2012. Local climate zones for urban temperature studies. Bull. Am. Meteorol. Soc. 93 (12), 1879–1900. https://doi.org/10.1175/BAMS-D-11-00019.1.

Wang, C., Middel, A., Myint, S.W., Kaplan, S., Brazel, A.J., Lukasczyk, J., 2018. Assessing local climate zones in arid cities: the case of Phoenix, Arizona and Las Vegas, Nevada. ISPRS J. Photogramm. Remote Sens. 141, 59–71. https://doi.org/10.1016/j.isprsjprs.2018.04.009.

Wang, Z.X., Song, J.Y., Chan, P.W., Li, Y.G., 2021. The urban moisture island phenomenon and its mechanisms in a high-rise high-density city. Int. J. Climatol. 41, E150–E170. https://doi.org/10.1002/joc.6672.

Wu, M.W., Luo, Y.L., Chen, F., Wong, W.K., 2019. Observed link of extreme hourly precipitation changes to urbanization over coastal South China. J. Appl. Meteorol. Climatol. 58 (8), 1799–1819. https://doi.org/10.1175/jamc-d-18-0284.1.

Yang, P., Ren, G., Hou, W., 2017a. Temporal–spatial patterns of relative humidity and the urban dryness island effect in Beijing City. J. Appl. Meteorol. Climatol. 56 (8), 2221–2237. https://doi.org/10.1175/JAMC-D-16-0338.1.

Yang, P., Ren, G., Yan, P., 2017b. Evidence for a strong association of short-duration intense rainfall with urbanization in the Beijing urban area. J. Clim. 30 (15), 5851–5870. https://doi.org/10.1175/JCLI-D-16-0671.1.

Yang, L., et al., 2018. A new generation of the United States National Land Cover Database: requirements, research priorities, design, and implementation strategies. ISPRS J. Photogramm. Remote Sens. 146, 108–123. https://doi.org/10.1016/j.isprsjprs.2018.09.006.

Yang, L., Smith, J., Niyogi, D., 2019a. Urban impacts on extreme monsoon rainfall and flooding in complex terrain. Geophys. Res. Lett. 46 (11), 5918–5927. https://doi.org/10.1029/2019gl083363.

Yang, Y., Smith, J., Yang, L., Baeck, M.L., Ni, G., 2019b. Regional impacts of urban irrigation on surface heat fluxes and rainfall in Central Arizona. J. Geophys. Res. Atmos. 124 (12), 6393–6410. https://doi.org/10.1029/2018JD030213.

Yang, P., Ren, G., Yan, P., Deng, J., 2021. Urbanization reduces frequency of light rain: an example from Beijing City. Theor. Appl. Climatol. https://doi.org/10.1007/s00704-021-03655-4.

Yoon, S.S., Lee, B., 2017. Effects of using high-density rain gauge networks and weather radar data on urban hydrological analyses. Water 9 (12). https://doi.org/10.3390/w9120931.

Zhang, Y.Z., Miao, S.G., Dai, Y.J., Bornstein, R., 2017. Numerical simulation of urban land surface effects on summer convective rainfall under different UHI intensity in Beijing. J. Geophys. Res.-Atmos. 122 (15), 7851–7868. https://doi.org/10.1002/2017jd026614.

Zhang, W., Villarini, G., Vecchi, G.A., Smith, J.A., 2018. Urbanization exacerbated the rainfall and flooding caused by hurricane Harvey in Houston. Nature 563 (7731), 384-+. https://doi.org/10.1038/s41586-018-0676-z.

Zhu, X.D., et al., 2019. Impact of urbanization on hourly precipitation in Beijing, China: spatiotemporal patterns and causes. Glob. Planet. Chang. 172, 307–324. https://doi.org/10.1016/j.gloplacha.2018.10.018.